Automatization of nanotomography

C. Dietz,[a),b)] S. Röper, and S. Scherdel
Chemische Physik, Technische Universität Chemnitz, D-09107 Chemnitz, Germany

A. Bernstein
Experimentelle Orthopädie, Martin-Luther-Universität Halle-Wittenberg, D-06097 Halle/Saale, Germany

N. Rehse and R. Magerle[a),c)]
Chemische Physik, Technische Universität Chemnitz, D-09107 Chemnitz, Germany

(Received 19 February 2007; accepted 8 April 2007; published online 3 May 2007)

An approach for automated nanotomography, a layer-by-layer imaging technique based on scanning probe microscopy (SPM), is presented. Stepwise etching and imaging is done *in situ* in a liquid cell of an SPM. The flow of etching and rinsing solutions after each etching step is controlled with solenoid valves which allow for an automated measuring protocol. The thermal drift and the drift of the piezo scanner is corrected by applying offsets calculated from the cross correlation coefficients between successive images. As an example, we have imaged human bone with ~10 nm resolution using tapping mode SPM and successive etching with hydrochloric acid. © *2007 American Institute of Physics.* [DOI: 10.1063/1.2736359]

I. INTRODUCTION

The invention of scanning probe microscopy (SPM) was a great success in imaging science.[1–4] Its limitation of imaging only surfaces of materials has been overcome with a layer-by-layer imaging technique called nanotomography[5] (Fig. 1) and with acoustic scanning probe microscopy.[6,7] SPM-based tomography methods are an interesting alternative to other high-resolution tomography methods such as electron[8–11] and x-ray tomography[12] since SPM-based methods require much simpler and cheaper setups. SPM-based nanotomography has been applied to different materials such as polymers[5,13,14] and metals[15] which have been imaged with ~10 nm resolution. In this work, the imaging process was quite time consuming because the sample had to be removed manually from the SPM for etching and had to be replaced for the next imaging step.

In this report we present an approach to automate this process. Imaging and etching is done in the liquid cell of a standard SPM instrument. Thermal drift is an intrinsic problem of SPM when one particular spot should be observed over a long period of time. Several approaches for correcting the sample drift have been applied in SPM and transmission electron microscopy, either by instrumentation[16] or with computational[17–21] based solutions. For instance, Mantooth *et al.*[19] have developed a fast image cross correlation algorithm for tracking single molecule motion on surfaces. We use the cross correlation technique to correct for the sample drift during the imaging process. As a result a series of 20 images can be obtained within 1 h. Combining our concept with high speed SPM imaging,[22–24] the total measuring time for one nanotomography volume image could be reduced to a few seconds.

II. CONCEPT FOR AUTOMATIZATION

The conventional approach for SPM-based nanotomography is divided into the following steps: First, an image of the desired material has to be captured with SPM. Second, the specimen had to be removed from the SPM with the aim of removing a few nanometer thick layer from the surface with an adequate erosion protocol, e.g., with wet-chemical etching,[14] plasma etching,[5,13] or chemomechanical polishing.[15] The next step was to remount the sample back to the SPM and to find the same position again. The smaller the region of interest the more difficult is the search for it. The traditional procedure is first to find a tagged position on the sample with an optical microscope integrated in the SPM and then to zoom into the interesting area by successively decreasing the scan size of the SPM. Hence, a lot of time is needed in scanning images and searching for the desired region. In best cases a data acquisition rate of approximately one layer per 30 min can be reached. A small rotational displacement cannot be excluded by this method, even if the specimen is aligned by a fixed border. Moreover, the sample plane might be tilted compared to the mounting done before.

All these efforts can be avoided when etching *in situ* in the SPM without removing the sample. A possible work flow for automated nanotomography is shown in Fig. 2. After capturing an image of the sample in water, the etching solution is flushed into the sealed liquid cell. Leaving the etchant in the liquid cell for a certain time, a layer with a thickness determined by the etching time is removed from the sample surface. The next step is flushing the liquid cell with, e.g., water, to stop the etching and to remove possible particles or generated residues on the surface. Then the next image can

[a)]Authors to whom correspondence should be addressed.
[b)]Electronic mail: christian.dietz@s2005.tu-chemnitz.de
[c)]Electronic mail: robert.magerle@physik.tu-chemnitz.de

 © 2007 American Institute of Physics

Downloaded 22 May 2008 to 10.1.150.91. Redistribution subject to AIP license or copyright; see http://rsi.aip.org/rsi/copyright.jsp

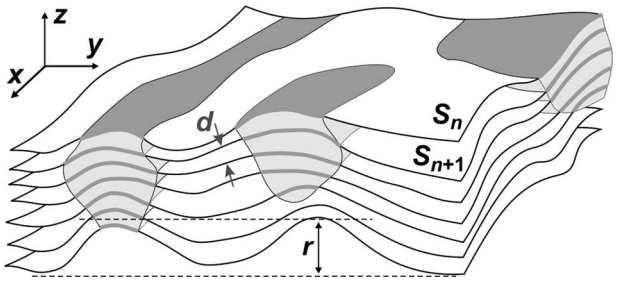

FIG. 1. Schematic illustration of the principle of nanotomography from a series of SPM images. The topography image $z_n(x,y)$ combined with an image of a physical property $P_n(x,y)$ of a material leads to a curved map $P_n(S_n)$ of the surface. By eroding the surface step by step, a stack of maps is obtained. The maps are aligned laterally and aligned by a distance d in z direction which corresponds to the mean etching rate. The result is a volume image of the physical property of the material. (From Ref. 5, © 2000 The American Physical Society).

be captured. The whole procedure (one etching and imaging cycle) will be repeated until the volume to be imaged has been eroded. The drift occurring between successive imaging steps is corrected by applying an appropriate offset calculated from the previously captured images. Figure 2 also indicates that ~3 min is necessary for one imaging and etching cycle, depending on the etching time. The tenfold increased data acquisition rate compared to the conventional nanotomography process is the great advantage of this method. Our concept is compatible with high speed SPM imaging[22–24] which could result in total measuring times of ~10 s for a volume image with ~100 slices.

A. Setup for *in situ* etching

We used a MultiMode™ SPM (Veeco Instruments Inc., Santa Barbara, USA) including a NanoScope IIIa Controller and NANOSCOPE software version 6.13 release 1. For imaging in water, we used a liquid cell (Veeco) consisting of glass, which allows for fast exchange of liquids. Figures 3(a) and 3(b) show a photograph of the SPM head displaying the liquid cell and a schematic sketch of it, respectively. A flexible sealing ring is placed between the liquid cell and the sample to obtain an enclosed volume. We used two of the ports as inlets and one as an outlet for the etching and flushing fluids. Figure 3(c) shows the entire setup for *in situ* etching. The liquid cell is connected with polyethylene tubes to three or more reservoirs (glass bottles), containing water, etchants, or other solutions. The solenoid valves of the type "2/2 way rocker" from Bürkert Fluid Control Systems (Ingelfingen, Germany) are attached to a serial relay card from Conrad Electronic (Hirschau, Germany). It is essential that all components of the etching device, which are directly in contact with aggressive acids and solvents are resistant against them. Otherwise, there is the danger of eroding material from the components of the setup, which in turn could cause unwanted consequences for the measurement (e.g., debris particles could contaminate the sample surface and change imaging conditions of the SPM).

The relay card is connected to the SPM computer and can be operated by individually programed etching protocols, implemented with NanoScript™ which is a part of the native SPM control software to communicate with the valves. Our NanoScript™ routines allow for different automated etching protocols such as switching between different etchants/solutions and flushing the liquid cell with water afterwards. Specific protocols can be developed for different samples.

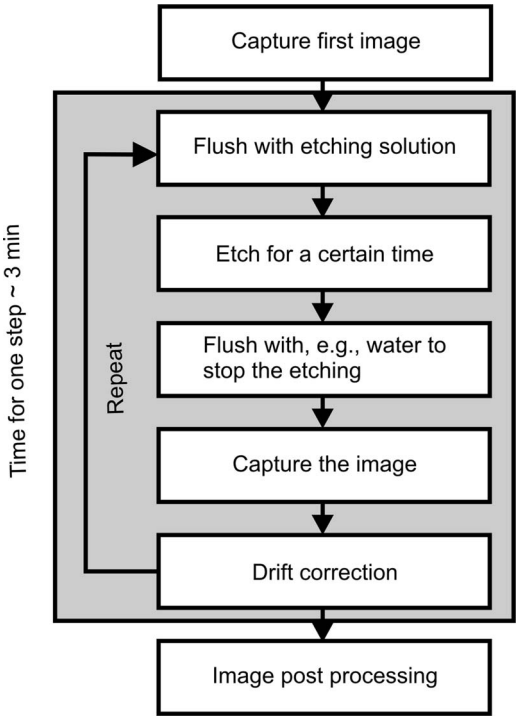

FIG. 2. Protocol for automated nanotomography. The step for etching away thin layers and capturing images (gray filled frame) can be repeated as long as required. See text for details.

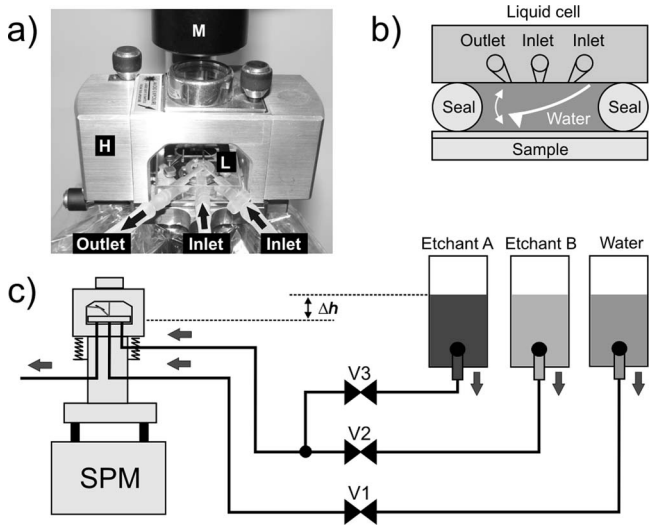

FIG. 3. (a) Photograph of the optical microscope (M) and measuring head (H) of a MultiMode™ SPM with the liquid cell (L) inserted and tubes connected to the inlets and outlets. (b) Schematic sketch of the liquid cell in contact with a sample sealed with a flexible silicone ring. This assembly yields a small closed volume with the probe inside. It can be filled with water or other solutions by using two of the three ports as inlets and one as an outlet. (c) Schematic illustration of the SPM and the etching device. The liquid cell is connected to several vessels. The flow rate through the cell is determined by the hydrostatic pressure given by the height difference Δh between the vessels and liquid cell. Solenoid valves (V1, V2, and V3) controlled with the SPM control software switch the different solutions.

Downloaded 22 May 2008 to 10.1.150.91. Redistribution subject to AIP license or copyright; see http://rsi.aip.org/rsi/copyright.jsp

This concept allows for two different kinds of etching methods. The first one is switching alternately between etchant and measuring medium (e.g., water or other solutions) to remove residues and particles from the sample surface after each etching step. In case of an etchant, which is optically transparent for the SPM laser, it is possible to combine etching and imaging by directly measuring in the etching solution, which is the second etching method. With a constant flow of the etchant through the liquid cell, there is also the opportunity of constantly removing residues and etched particles from the surface. Since there is no disengagement of the tip from the sample, a loss of the considered spot on the surface is unlikely. However, the small flow rate through the liquid cell, which is applied to avoid disturbances during imaging, may lead to more contamination by residuals on the surface. Finally, it depends on the specific material and etching technique which combination of methods and parameters fits best.

B. Drift correction

For nanotomography it is essential to observe the same area on the sample surface during imaging and etching. Even though post processing methods, which correct for displacements between successive images,[25–27] are applicable to a measured stack of images, a better approach is to avoid or minimize them during the measurement. Afterwards, post processing techniques can still be utilized to remove residual displacements and distortions.

We have applied an algorithm to maintain the same position on the sample surface. The basic idea is to calculate the cross correlation coefficient between two successive images[26] and to correct for the offset. One image is considered as a reference and is compared with a second image, the template. Both images might be shifted due to the described drift. Aiming to correct for this displacement, a reference area containing distinctive features is chosen in the reference image. The size and position of the reference area and the searching area can be individually defined by the user. One has to consider the necessary computing time, which means that the larger the reference area and the searching area the more time consuming is the calculation of the cross correlation coefficient.[28]

For successive imaging it is first necessary to capture two images with the SPM. The offset between the two images is calculated as described and is applied by the control software. The emerging drift can be compensated by continuously repeated capture and calculation of the offset.

Our drift correction algorithm offers the opportunity to choose either a fixed reference image or to vary it during a measurement. In the first case, all further captured images will be correlated with the same image as the reference. This approach will only be successful if the sample surface does not change too much during one etching step. Otherwise the cross correlation coefficient for the two images results in a wrong value. In general, however, the sample surface is stepwise eroded and hence the structure changes only slightly with time. Furthermore, the success of the drift correction depends crucially on the image quality. If the imaging parameters change drastically or the reference area does not contain a characteristic feature (e.g., a defect), this method fails. The consequence is an applied offset to the piezoelectric scanner which jumps remarkably compared to previous offsets. For this reason, we discard correction values which are larger than half of the diameter of the searching area. Our drift compensation was implemented in C++ and converted into a dynamic link library executable by the SPM control software NANOSCOPE.

C. Imaging in liquids

The possibility of imaging surfaces in liquids turned the SPM into an attractive tool for the study of liquid-solid interfacial phenomena and the observation of processes in their natural biological environment. Tapping mode atomic force microscopy (TM-AFM) in liquids,[29,30] however, differs in the choice of imaging parameters in contrast to TM-AFM in air. The structural design of the liquid cell and the mechanical coupling of the liquid cell to the cantilever and to the etching device make it difficult to identify the cantilever's vibration spectrum. In our experiments the cantilever's fundamental eigenmode ($\sim$9 kHz) gave no adequate phase contrast, but a higher eigenmode with a frequency of $\sim$113 kHz did.[31] This specific frequency of the cantilever makes it possible to image in the repulsive regime[32] leading to stable oscillation conditions.

We used triangular shaped Si_3N_4 cantilevers (Veeco) with two tips on each side of the cantilever substrate, which turned out to be the most effective and stable conformation for operation in water. We used the cantilever with a spring constant of $k=0.58$ N/m. The not needed cantilever on the same side of the substrate was removed in order to avoid touching the specimen with this tip. Cantilevers with drastically higher or lower spring constants proved to be not suited for our particular application and specimen. Because of the reduced Q factor ($Q\approx 30$), the phase contrast between the different phases in heterogeneous material is much lower.[33] The best image quality in water was achieved using a free rms amplitude of the cantilever $A_0=30-40$ nm and an amplitude setpoint $A/A_0\approx 0.6$. In most cases of the imaged bone specimens the total number of layers is limited by the detoriating image quality of phase images. We believe that this effect is caused by contaminations of the tip or particles or residues generated during the etching process.

D. Post processing

After data acquisition the series of images were postprocessed and combined to volume images like in previous work.[14,27] This includes flattening, contrast enhancement, nonlinear image registration, and visualization with AMIRA® (Mercury™ Computer Systems Inc., Mountain View, USA).

E. Sample preparation

The bone samples were thin sections which have been prepared using standard procedures.[34,35] Parts of the compact bone of the human femur were cut into small pieces with different orientations with respect to the osteons and dehydrated with ethanol solutions with an increasing concentration series for 24 h. In addition, the samples were defatted

Downloaded 22 May 2008 to 10.1.150.91. Redistribution subject to AIP license or copyright; see http://rsi.aip.org/rsi/copyright.jsp

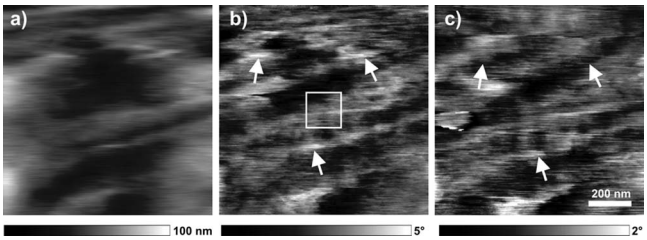

FIG. 4. (a) TM-AFM height and (b) phase images of human bone at the beginning of our measurement and (c) phase image after 18 etching steps captured in water. Bright parts in the phase image correspond to a high phase signal whereas the dark regions are related to a low phase signal. In both images the same spot of the surface can be recognized. Also a change in the structure is visible, indicated by the white arrows. The bright frame shows the position and the size of the reference area chosen for the calculation of the displacement of successive images.

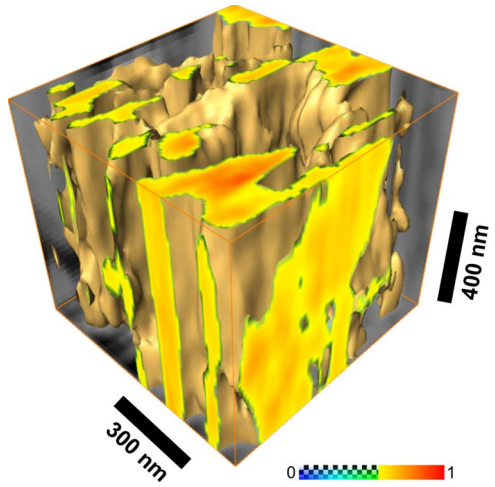

FIG. 5. (Color online) Three dimensional isosurface of a volume phase image ($256\times256\times19$ voxels) of human bone. The image was captured using automated nanotomography within 1 h and consists of 19 layers. The phase signal is normalized to the range from 0 to 1 and the threshold of the isosurface is set to 0.62 (see color bar). The faces of the boundary box are colored according to the corresponding phase values.

with Roticlear® (Carl Roth GmbH & Co. KG, Karlsruhe, Germany) which also served as a clearing medium, embedded in polymethylmethacrylate (Merck KGaA, Darmstadt, Germany), sectioned into 5 μm thick slices using a microtome, and fixed onto a silicon substrate.

F. Etching protocol

We used a 0.1*M* hydrochloric acid as an etchant. Thin films of ~80 nm were removed from the sample surface by filling the liquid cell with the etchant and exposing the sample to it for 30 s. To stop the etching, the liquid cell was flushed with water. In order to remove residues from the sample surface, we applied a high flow rate of water (~10 ml/min). Afterwards, we switched to a smaller flow rate of water (~1 ml/min) through the cell to avoid diffusion of the etchant into the liquid cell during the imaging process. The whole protocol was executed automatically without user intervention. Only the amplitude setpoint A/A_0 was decreased manually in some cases of losing the contact between tip and surface.

The etching rate was determined similar to that described in Ref. 36. A specimen was cut into two pieces, of which one was covered with a gold layer. Afterwards the two pieces were glued together again. The sample was planarized by cutting it perpendicularly to the gold layer and polishing. The gold layer acts as an inert height reference during the etching procedure. Etching with 0.1*M* HCl for 30 s removes a layer of ~80 nm.

III. RESULTS AND DISCUSSION

A. Maintaining the image position with the drift correction algorithm

Our aim in this study was to reconstruct a volume image of human bone with automated nanotomography. For this purpose we observed the same spot of the surface during the whole nanotomography measurement using our drift correction algorithm. Figure 4 shows a height image (a) and two typical phase images [(b) and (c)] of the same spot of a human bone sample after different etching steps. A characteristic distribution of the phase signal can be observed. This phase signal can be related to the mechanical properties of the surface.[37–39]

The bright frame in Fig. 4(b) indicates the reference area chosen for the calculation of the displacement. The position of the 40×40 pixels^2 large area was selected such that it contains a region with distinct features and good contrast. The sample surface was observed for 67 min with a scan rate of 2 Hz and a resolution of 256×256 pixels^2. The tip was withdrawn and engaged for each etching step, resulting in an additional displacement. Since the surface changes during the etching process the reference image was chosen variable as described in the previous section. The cross correlation coefficient was calculated from the phase image. Figure 4(c) shows changes compared to Fig. 4(a) caused by the etching progress. The temporal development of the displacement (not shown) is irregular, similar to Ref. 19. We like to emphasize that the final displacement, which was 2.109 μm in the x direction and 4.992 μm in the y direction after 19 images, exceeded the scan size of our measurement several times and was successfully corrected by our drift correction algorithm. This shows that our algorithm works well even for changing surface structures. Furthermore, this drift correction can be successfully used during the imaging of dynamic processes on surfaces, such as the microdomain dynamics of block copolymers similar to Refs. 40 and 41 or during the observation of the crystal growth of semicrystalline polypropylene, similar to Refs. 42 and 43. As long as there are enough distinctive features on the surface within the reference area, our algorithm corrects successfully for the drift.

B. Obtained volume image using the etching device

Figure 5 shows a volume phase image ($256\times256\times19$ pixels^3) of human bone, obtained with automated *in situ* etching and imaging. The TM-AFM height and phase images were postprocessed with linear and nonlinear image registration as described in Sec. II D. For each layer the phase values have been allocated to the corresponding height map of the imaged area leading to a series of curved maps (Fig. 1). A volume image is reconstructed by stacking these

Downloaded 22 May 2008 to 10.1.150.91. Redistribution subject to AIP license or copyright; see http://rsi.aip.org/rsi/copyright.jsp

curved maps with a mutual distance corresponding to the average etching depth. With the given threshold, bright regions having a high phase signal were separated from dark areas having lower phase signals. The latter regions appear transparent in the volume image. The interpretation of the imaged specimen structure is beyond the scope of this article. The image size was restricted to 19 layers due to the decreasing image quality during the measurement. Possible reasons include residues on the surface or contaminations of the SPM tip. The acquisition time for the shown volume image was about 1 h, which is ten times faster than comparable measurements of volume images of other materials prepared by nonautomated nanotomography.

C. Summary and outlook

We have developed an etching device for automated nanotomography based on SPM. The setup allows for imaging and etching in liquids with a data acquisition rate of ~3 min per layer and includes drift correction based on image analysis. The setup is based on a standard SPM which was extended with a custom built liquid handling system and extensions of the SPM control software. We have demonstrated the method by imaging human bone.

The acquisition rate could be further increased by imaging directly in the liquid cell with the etchant as imaging medium under a defined flow rate. Our etching system is also compatible with high speed SPM imaging[22–24] which could lead to a total measuring time of a few seconds for one nanotomography image. Our concept is not limited to bone and polymeric materials but could also be used to image metals, ceramics, semiconductors, as well as composite materials. In addition, our etching device can be easily extended to electrochemical etching.[15] Furthermore, the adjustment of imaging parameters could be automated and the often detoriating imaging quality might be improved by introducing additional cleaning cycles.

ACKNOWLEDGMENTS

This work was financially supported by the European Commission (FORCETOOL, NMP4-CT-2004-013684) and the VolkswagenStiftung. The authors would like to thank C. Vetter for help with the sample preparation.

[1] G. Binnig, H. Rohrer, Ch. Gerber, and E. Weibel, Phys. Rev. Lett. **49**, 57 (1982).
[2] G. Binnig, C. F. Quate, and Ch. Gerber, Phys. Rev. Lett. **56**, 930 (1986).
[3] S. Magonov and M. Whangbo, *Surface Analysis with STM and AFM* (VCH, Weinheim, 1996).
[4] R. Wiesendanger, *Scanning Probe Microscopy* (Springer, Berlin, 1998).
[5] R. Magerle, Phys. Rev. Lett. **85**, 2749 (2000).
[6] R. A. Lemons and C. F. Quate, Appl. Phys. Lett. **24**, 163 (1974).
[7] K. Raum, I. Leguerney, F. Chandelier, M. Talmant, A. Saïed, F. Peyrin, and P. Laugier, Phys. Med. Biol. **51**, 733 (2006).
[8] W. A. Gaunt and P. N. Gaunt, *Three Dimensional Reconstruction in Biology* (Pitman, Kent, 1978).
[9] W. J. Landis, M. J. Song, A. Leith, L. McEwen, and B. F. McEwen, J. Struct. Biol. **110**, 39 (1993).
[10] W. J. Landis, K. J. Hodgens, J. Arena, M. J. Song, and B. F. McEwen, Microsc. Res. Tech. **33**, 192 (1996).
[11] J. Frank, *Three-Dimensional Electron Microscopy of Macromolecular Assemblies* (Academic, San Diego, 1996).
[12] T. Ohgaki *et al.*, Adv. Eng. Mater. **8**, 473 (2006).
[13] M. Konrad, A. Knoll, G. Krausch, and R. Magerle, Macromolecules **33**, 5518 (2000).
[14] N. Rehse, S. Marr, S. Scherdel, and R. Magerle, Adv. Mater. (Weinheim, Ger.) **17**, 2203 (2005).
[15] M. Göken, R. Magerle, M. Hund, and K. Durst, Prakt. Metallogr. **35**, 257 (2004).
[16] D. W. Pohl and R. Möller, Rev. Sci. Instrum. **59**, 840 (1988).
[17] V. Y. Yurov and A. N. Klimov, Rev. Sci. Instrum. **65**, 1551 (1994).
[18] R. Staub, D. Alliata, and C. Nicolini, Rev. Sci. Instrum. **66**, 2513 (1995).
[19] B. A. Mantooth, Z. J. Donhauser, K. F. Kelly and P. S. Weiss, Rev. Sci. Instrum. **73**, 313 (2002).
[20] B. Mokaberi and A. A. G. Requicha, *Proceedings of the 2004 IEEE International Conference on Robotics and Automation* (IEEE Computer Society, Washington, DC, 2004), p. 416.
[21] B. Schaffer, W. Grogger, and G. Kothleitner, Ultramicroscopy **102**, 27 (2004).
[22] T. Ando, N. Kodera, E. Takai, D. Maruyama, K. Saito, and A. Toda, Proc. Natl. Acad. Sci. U.S.A. **98**, 12468 (2001).
[23] J. K. Hobbs, C. Vasilev, and A. D. L. Humphris, Analyst (Cambridge, U.K.) **131**, 251 (2006).
[24] A. D. L. Humphris, M. J. Miles, and J. K. Hobbs, Appl. Phys. Lett. **86**, 034106 (2005).
[25] K. Henriksen and S. L. S. Stipp, Am. Mineral. **87**, 5 (2002).
[26] J. Garnaes, L. Nielsen, K. Dirscherl, J. F. Jørgensen, J. B. Rasmussen, P. E. Lindelof, and C. B. Sørensen, Appl. Phys. A: Mater. Sci. Process. **66**, 831 (1998).
[27] S. Scherdel, S. Wirtz, N. Rehse, and R. Magerle, Nanotechnology **17**, 881 (2006).
[28] K. D. Tönnies, *Grundlagen der Bildverarbeitung* (Pearson Studium, München, 2005).
[29] P. K. Hansma *et al.*, Appl. Phys. Lett. **64**, 1738 (1994).
[30] J. Legleiter and T. Kowalewski, Appl. Phys. Lett. **87**, 163120 (2005).
[31] R. W. Stark, T. Drobek, and W. M. Heckl, Appl. Phys. Lett. **74**, 3296 (1999).
[32] R. García and R. Pérez, Surf. Sci. Rep. **47**, 197 (2002).
[33] T. R. Rodríguez and R. García, Appl. Phys. Lett. **82**, 4821 (2003).
[34] P. Böck, *Romeis Mikroskopische Technik* (Urban und Schwarzenberg, München, 1989).
[35] H. A. Yuehuei and K. L. Martin, *Handbook of Histology Methods for Bone and Cartilage* (Humana, Totowa, 2003).
[36] G. W. Marshall, Jr., I. C. Wu-Magidi, L. G. Watanabe, N. Inai, M. Balooch, J. H. Kinney, and S. J. Marshall, J. Biomed. Mater. Res. **42**, 500 (1998).
[37] J. P. Cleveland, B. Anczykowski, A. E. Schmid, and V. B. Elings, Appl. Phys. Lett. **72**, 2613 (1998).
[38] R. García, J. Tamayo, and A. S. Paulo, Surf. Interface Anal. **27**, 312 (1999).
[39] R. García, C. J. Gómez, N. F. Martínez, S. Patil, C. Dietz, and R. Magerle, Phys. Rev. Lett. **97**, 016103 (2006).
[40] A. Knoll, K. S. Lyakhova, A. Horvart, G. Krausch, G. J. A. Sevink, A. V. Zvelindovsky, and R. Magerle, Nat. Mater. **3**, 886 (2004).
[41] L. Tsarkova, A. Knoll, and R. Magerle, Nano Lett. **6**, 1574 (2006).
[42] H. Schönherr, R. M. Waymouth, and C. W. Frank, Macromolecules **36**, 2412 (2003).
[43] J.-J. Zhou, J.-G. Liu, S.-K. Yan, J.-Y. Dong, L. Li, C.-M. Chan, and J. M. Schultz, Polymer **46**, 4077 (2005).

Downloaded 22 May 2008 to 10.1.150.91. Redistribution subject to AIP license or copyright; see http://rsi.aip.org/rsi/copyright.jsp